Wireless Charger Placement and Power Allocation for Maximizing Charging Quality

Sheng Zhang, *Member, IEEE*, Zhuzhong Qian, *Member, IEEE*, Jie Wu, *Fellow, IEEE*, Fanyu Kong, and Sanglu Lu, *Member, IEEE*

Abstract—Wireless power transfer is a promising technology used to extend the lifetime of, and thus enhance the usability of, energy-hungry battery-powered devices. It enables energy to be wirelessly transmitted from power chargers to energy-receiving devices. Existing studies have mainly focused on maximizing network lifetime, optimizing charging efficiency, minimizing charging delay, etc. In this paper, we consider wireless charging service provision in a two-dimensional target area and focus on optimizing charging quality, where the power of each charger is adjustable. We first consider the charger Placement and Power allocation Problem with Stationary rechargeable devices (SP^3): Given a set of stationary devices and a set of candidate locations for placing chargers, find a charger placement and a corresponding power allocation to maximize the charging quality, subject to a power budget. We prove that SP^3 is NP-complete, and propose an approximation algorithm. We also show how to deal with mobile devices (MP^3), cost-constrained power reconfiguration (CRP), and optimization with more candidate locations. Extensive simulation results show that, the proposed algorithms perform very closely to the optimum (the gap is no more than 4.5, 4.4, and 5.0 percent of OPT in SP^3, MP^3, and CRP, respectively), and outperforms the baseline algorithms.

Index Terms—Wireless power transfer, charger placement, power allocation, submodularity, approximation algorithm

1 Introduction

Over the past few years, wireless portable devices greatly improved the quality of our lives. Due to the limited battery capacity of these devices, they can only remain operational for a limited amount of time before connecting wired chargers. To extend the lifetime of these battery-powered devices, solutions from different perspectives have been proposed, including energy harvesting [1], [2], [3], energy conservation [4], [5], battery replacement [6], etc. However, energy harvesting remains limited in practice due to its partial predictability and the large size of harvesting panels; energy conservation cannot compensate for depletion; battery replacement is costly and impractical.

Wireless power transfer provides a promising alternative that has attracted significant attention from both academia and industry. Kurs et al. experimentally demonstrated that energy can be efficiently transmitted between magnetically resonant objects without any interconnecting conductors [7]. This technology has led to the development of several commercial products, e.g., Intel developed the wireless identification and sensing platform (WISP) for battery-free monitoring [8]; more than 30 types of popular phones are beginning to embrace wireless charging [9]; and even vehicles [10] and unmanned planes [11] are now supporting wireless charging. It is predicted that the wireless charging market will be worth $13.78 billion by 2020 [12].

Existing studies regarding this issue have mainly focused on maximizing the lifetime of the underlying network [13], optimizing the efficiency of charging scheduling [14], energy provisioning [15], collaboration between chargers [16], minimizing total charging delay [17], minimizing maximum radiation point [18], etc.

In contrast to existing works, we consider how to efficiently provide wireless charging service [22]. Suppose a service provider decides to offer a wireless power charging service in a two-dimensional (2-D) target area, e.g., a campus or park. Based on historical data analysis and market investigation, it could predict the location or trajectory information of potential customers (i.e., devices) and then preselect a certain number of candidate locations for placing wireless power chargers (chargers for short in the sequel), the power of which is adjustable. Given a power budget, the provider wants to maximize its revenue, which is proportional to the charging quality defined later in the paper. In order to maximize the charging quality, a limited number of chargers with appropriate power levels must be strategically placed at a subset of the candidate locations.

In this paper, we consider the charger Placement and Power allocation Problem with Stationary devices (SP^3): *Given a set of stationary devices and a set of candidate locations for placing chargers, how to find a charger placement and a corresponding power allocation to maximize the charging quality,*

- *S. Zhang, Z.Z. Qian, and S.L. Lu are with the State Key Laboratory for Novel Software Technology, Nanjing University, Nanjing 210023, China. E-mail: {sheng, qzz, sanglu}@nju.edu.cn.*
- *J. Wu is with the Center for Networked Computing, Temple University, Philadelphia, PA 19122. E-mail: jiewu@temple.edu.*
- *F.Y. Kong is with Ant Financial, Hangzhou, Zhejiang 310013, China. E-mail: njukongfy@gmail.com.*

Manuscript received 2 July 2015; revised 15 Sept. 2017; accepted 2 Nov. 2017. Date of publication 8 Nov. 2017; date of current version 3 May 2018. (Corresponding author: Sheng Zhang.)
For information on obtaining reprints of this article, please send e-mail to: reprints@ieee.org, and reference the Digital Object Identifier below.
Digital Object Identifier no. 10.1109/TMC.2017.2771425

TABLE 1
Comparison of Near-Field WPT Standards

Standards	Charging Technology	Efficiency	Distance	Communication Frequency	Power Frequency	Key Supporters
Wireless Power Consortium (Qi) [19]	Magnetic Induction	High	Short	100 to 205 khz	100 to 205 khz	HTC, Nokia, Sony, Verizon Wireless
Power Matters Alliance (Powermat) [20]	Magnetic Induction	High	Short	277 to 357 khz	277 to 357 khz	AT&T, Duracell, Starbucks
Alliance for Wireless Power (WiPower) [21]	Magnetic Resonance	Medium	Medium	2.4 GHz	6.78 Mhz	Witricity, Intel

subject to a power budget. We prove that SP^3 is NP-complete by reduction from the set cover problem [23]. To design an approximation algorithm for SP^3, we first consider two special cases of SP^3. The algorithms for these special cases help us design the final algorithm, namely, TCA, for SP^3, with an approximation factor of $\frac{1-1/e}{2L}$, where e is the base of the natural logarithm, and L is the maximum power level.

We provide three extensions of SP^3. First, we extend SP^3 to MP^3 where rechargeable devices are mobile. We leverage discrete time modeling to represent the trajectory of each device, and then we tailor the algorithm for SP^3 to MP^3. Second, mobile devices may leave or enter the target area, which makes the current charger placement and power allocation not optimal in terms of charging quality. We may need to compute a new charger placement and power allocation. However, switching from one power allocation to another incurs some reconfiguration cost. We thus study the cost-constrained reconfiguration problem (CRP), and design an approximation algorithm of factor $\frac{(1-1/e)F}{4BL}$, where B is the power budge and F is the reconfiguration cost threshold. Third, we show how to deal with the case in which chargers are allowed to be placed at any location within the target area, and evaluate how the overall charging quality evolves as the number of candidate locations increases.

Simulation results show that, the proposed algorithms perform very closely to the optimum (the gap is no more than 4.5, 4.4, and 5.0 percent of OPT in SP^3, MP^3, and CRP, respectively), and outperforms the baseline algorithms.

The contributions of this paper are three-fold:

- To the best of our knowledge, we are the first to study the joint optimization of charger placement and power allocation problem. We present a formal problem statement and prove that it is NP-complete.
- We propose an approximation algorithm, i.e., TCA, for SP^3. Based on TCA, we provide solutions for mobile devices, cost-constrained reconfiguration, and more candidate locations.
- Evaluations are conducted to confirm the effectiveness and advantages of the proposed algorithms.

The rest of the paper is organized as follows. We discuss background and related work in Section 2. We introduce the SP^3 problem in Section 3. We present our solutions to SP^3 in Section 4. We provide several extensions in Section 5. Before we conclude the paper in Section 7, we evaluate our design in Section 6.

2 Background and Related Work

2.1 Wireless Power Transfer: A Primer

The limited battery capacity of mobile devices has created a demand for more convenient and accessible ways to charge them. Previous solutions including harvesting energy from environment [2], [3] and energy conservation [4], [5] are either unstable or not able to compensate for energy depletion. Wireless power transfer (WPT) is then proposed as a promising technology to fulfill the needs of mobile devices.

Nikola Tesla conducted the first experiment in wireless power transfer as early as the 1890s: an incandescent light bulb was successfully powered using a coil receiver that was in resonance with a nearby magnifying transmitter [24]. Recently, Kurs et al. experimentally demonstrated that energy can be efficiently transmitted between magnetically resonant objects without any interconnecting conductors, e.g., powering a 60 W light bulb, which is two meters away, with approximately 40 percent efficiency [7]. Today, examples of wireless charging systems include rechargeable toothbrushes, biomedical implants, Tesla motors, etc.

In general, WPT techniques mainly fall into two categories, non-radiative (near-field) and radiative (far-field). In near-field WPT techniques, there are three main standards, listed in Table 1. The Qi open standard [19] was released by Wireless Power Consortium in 2009. Since then, over 900 Qi-compliant devices have become available. Powermat [20] and WiPower [21] are released in 2012 by Power Matters Alliance and Alliance for Wireless Power, respectively. We see from Table 1 that, Qi and Powermat are similar in terms of distance and frequency, while WiPower allows a medium charging distance. In far-field WPT techniques, power is transferred by beams of electromagnetic radiation. These techniques can transport energy over longer distances but must be aimed at the receiver. Examples include WISP [8] and WiPoT [25].

For near-filed WPT standards, the power frequency is usually very small compared with today's WLAN or cellular frequencies. For far-field standards, currently, there no special frequency band for them. Hence, the time division dulplex WPT (TDD-WPT) [26] was proposed to enable the coexistence of WPT and wireless communication. Many existing works [13], [27], [28] on charging scheduling also assume that wireless communication and charging can coexist without any interfere. For example, energy charging is carried out in the 903-927 MHz band while communication uses the 2.4 GHz band in [13].

For more details, please refer to [29].

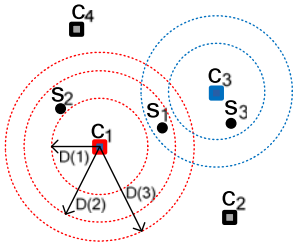

Fig. 1. Example of chargers, devices, and power levels. The maximum cover distance of a power level is indicated by the radius of a dashed circle.

2.2 Related Work

There is a number of studies that inspire our work. We can classify them into two broad types according to whether the wireless charger is stationary or mobile.

When the wireless chargers are static, a charger placement framework is proposed in [15] to ensure that each device receives sufficient energy for continuous operation. The joint optimization of charger placement and power allocation is considered in [22]. How to obtain the maximum electromagnetic radiation point in a given plane is studied in [18]. The performance of multi-device simultaneous charging is investigated in [30].

For mobile wireless chargers, existing studies have considered various decision variables and objectives. To maximize network lifetime, charging sequence and packet routing are optimized in [13], [31], while charger velocity is optimized in [32]. To maximize the ratio of the charger's vacation time (i.e., time spent at the home service station) over the cycle time, travelling path and stop schedules are optimized in [14], [33]. To maximize energy usage effectiveness, collaboration between mobile chargers is optimized in [16], [34]. To minimize the total charging delay, stop locations and durations are optimized in [17]. NDN-based energy monitoring and reporting protocols are designed in [28] with a special focus on scheduling mobile chargers for multiple concurrent emergencies. To simultaneously minimize charger travel distance and charging delay, synchronized charging sequences based on multiple nested tours are optimized in [35]. Given heterogeneous charging frequencies of sensors, how to schedule multiple charging rounds to minimize total moving distance of mobile chargers is studied in [36]. Given a set of candidate charging itineraries, how to select itineraries and determine a corresponding charging association to minimize the amount of overhead energy is considered in [37]. Different from them, our work jointly determines charger placement and power allocation to improve the charging quality, subject to a budget constraint.

3 Problem

In this section, we first introduce the wireless charging model (Section 3.1), then we present the problem (Section 3.2).

3.1 Wireless Charging Model

We consider wireless charging service provision using stationary chargers in this paper. The two-dimensional target area under consideration contains a set of M stationary rechargeable devices $\mathcal{S} = \{s_1, s_2, \ldots, s_M\}$. These devices could be RFIDs [8], sensors [13], phones [9], vehicles [10], drones [11], etc. The location $(x[s_j], y[s_j])$ of a device s_j can be localized using existing techniques (e.g., [38]) or GPS and is reported to the wireless charging service provider via long-distance communications. Based on historical data analyses, market investigation, and urban planning, the service provider could preselect a certain number of candidate locations for placing chargers. These locations are denoted by a set $\mathcal{C} = \{c_1, c_2, \ldots, c_N\}$. The coordinate of c_i is $(x[c_i], y[c_i])$. Without causing confusion, we also use c_i to denote the charger placed at candidate location c_i.

The distance function $d(\cdot, \cdot)$ gives the Euclidean distance between two objects (chargers or devices), e.g., the distance between charger c_i and device s_j is

$$d(c_i, s_j) = \sqrt{(x[c_i] - x[s_j])^2 + (y[c_i] - y[s_j])^2}. \tag{1}$$

Fig. 1 shows an example of chargers, devices, and power levels. There are four candidate locations, i.e., $\mathcal{C} = \{c_1, c_2, c_3, c_4\}$, and three devices, i.e., $\mathcal{S} = \{s_1, s_2, s_3\}$.

For wireless chargers, we assume that the power of each charger is adjustable [18]. Each charger can be operated at L different power levels. Denote the power of charger c by p; without loss of generality, we define

$$p = h \cdot p_{\min}, \tag{2}$$

where $h \in \{1, 2, \ldots, L\}$ is the power level of charger c, and $p_{\min}$ is the constant gap between two adjacent power levels. Note that, this kind of discretization is for simplicity. As long as the number of allowable power levels of each charger is finite, the proposed algorithms are still feasible.

We assume an omnidirectional charging model which is widely adopted in existing studies [15], [17], [18], [32]. In this model, the receiving power at rechargeable devices is determined by the transmission power of a charger and the distance between a device and a charger. According to the profiling experiments in [15], the power $p(c_i, s_j)$ received by device s_j from charger c_i can be captured by the follow model

$$p(c_i, s_j) = \begin{cases} \frac{\alpha \cdot p_i}{(d(c_i, s_j) + \beta)^2} & d(c_i, s_j) \le D(h_i) \\ 0 & d(c_i, s_j) > D(h_i), \end{cases} \tag{3}$$

where α and β are known constants determined by hardware of chargers and devices and the environment, and $D(h_i)$ is the maximum cover distance of a charger with power level h_i. We further assume that, a charger can transfer energy to multiple devices simultaneously without significantly reducing the received power at each device [30].

When a device is far away from a charger, the device receives negligible power that cannot be rectified to useful electrical energy. The threshold of this negligible power is denoted by p_{th}. By letting $\frac{\alpha \cdot p_i}{(D(h_i) + \beta)^2} = p_{th}$, we have

$$D(h_i) = \sqrt{\frac{\alpha \cdot h_i \cdot p_{min}}{p_{th}}} - \beta. \tag{4}$$

That is, given constants α, β, and p_{th}, the maximum coverage radius $D(h_i)$ of a charger c_i is determined by its power level h_i. In Fig. 1, when we place a charger c_1 with a power level h_1 being 1, its maximum coverage radius is $D(1)$, and

thus c_1 cannot transfer power to s_1, which is more than $D(1)$ distance away from c_1.

Denote by $\mathcal{R}$ a charger placement, where $\mathcal{R}$ is a subset of $\mathcal{C}$, and denote by a vector $\mathbf{H} = (h_1, h_2, \ldots, h_N)$ a power allocation. As we know, the power received by one device from multiple chargers is additive [15]. Therefore, given a charger placement $\mathcal{R}$ and a power allocation $\mathbf{H}$, the total power $p_{\mathcal{R},\mathbf{H}}(s_j)$ received by device s_j is

$$p_{\mathcal{R},\mathbf{H}}(s_j) = \sum_{c_i \in \mathcal{R}} p(c_i, s_j). \tag{5}$$

For example, in Fig. 1, if we set $\mathcal{R} = \{c_1, c_3\}$ and $\mathbf{H} = (2, 0, 2, 0)$; we have $p_{\mathcal{R},\mathbf{H}}(s_1) = p(c_1, s_1) + p(c_2, s_1)$, $p_{\mathcal{R},\mathbf{H}}(s_2) = p(c_1, s_2)$, and $p_{\mathcal{R},\mathbf{H}}(s_3) = p(c_2, s_3)$.

3.2 Problem Formulation

The energy consumption rate of a device may fluctuate over time. Similar to [15], we define the average energy consumption rate of a device as follows. Taking a sensor for example, denote the energy consumption rate for sensing/logging and sleeping by p_a and p_s, respectively. Assuming the cycle is T and the time duration for sensing/logging is T_a, then the average energy consumption rate of this sensor is $P = \frac{p_a \cdot T_a + p_s \cdot (T - T_a)}{T}$. If the total power received by the sensor is no less than P, then it can sustain its operations over time and the over-received energy would be useless.[1]

Based on this, we now give the definition of charging quality. Denote the average energy consumption rate of s_j by P_j. The charging quality $Q_{\mathcal{R},\mathbf{H}}(s_j)$ with respect to $\mathcal{R}$ and $\mathbf{H}$ on device s_j is

$$Q_{\mathcal{R},\mathbf{H}}(s_j) = \min\{p_{\mathcal{R},\mathbf{H}}(s_j), P_j\}, \tag{6}$$

where $p_{\mathcal{R},\mathbf{H}}(s_j)$ is the total power received by device s_j.

We define our objective function as follows:

Definition 1 (Charging Quality). *Given a charger placement $\mathcal{R}$ and a power allocation $\mathbf{H}$, the charging quality, denoted as $Q(\mathcal{R}, \mathbf{H})$, is defined as the sum of the charging qualities of over all devices with respect to $\mathcal{R}$ and $\mathbf{H}$, i.e., $Q(\mathcal{R}, \mathbf{H}) = \sum_{j=1}^{M} Q_{\mathcal{R},\mathbf{H}}(s_j)$.*

The SP^3 problem studied in this paper is:

Problem 1 (Charger Placement and Power Allocation Problem with Stationary Devices, SP^3). *Given a set $\mathcal{C}$ of candidate locations, a set $\mathcal{S}$ of devices, and a power budget B, SP^3 is to find a charger placement $\mathcal{R}$ and a power allocation $\mathbf{H}$ to maximize $Q(\mathcal{R}, \mathbf{H})$, subject to the power budget constraint, i.e., $\sum_{c_i \in \mathcal{R}} p_i \leq B$.*

By reducing the NP-complete Set Cover problem (SC) [23] to SP^3, we have the following theorem.

Theorem 1. *SP^3 is NP-complete.*

Proof. The decision version of the SC problem is as follows: Given a universe $\mathcal{U} = \{e_1, e_2, \ldots, e_m\}$ of m elements and an integer y, a collection of subsets of $\mathcal{U}$, $\mathcal{V} = \{\mathcal{V}_1, \mathcal{V}_2, \ldots, \mathcal{V}_k\}$, does there exist a sub-collection of $\mathcal{V}$ of size y that covers all elements of $\mathcal{U}$?

Given an instance of the decision version of the SC problem, we construct an instance of the SP^3 problem as follows. We let $L = 1$, i.e., every charger can only be operated at the fixed power $p_{\min}$. For each element e_j in $\mathcal{U}$, we construct a device s_j in SP^3. We assume that all devices have the same maximum power consumption rate, i.e., $P_1 = P_2 = \ldots, = P_m = P$. For each $\mathcal{V}_i \in \mathcal{V}$, we add a candidate location c_i to SP^3. For each element e_j in $\mathcal{V}_i$, we move s_j into the coverage of c_i. We also make sure that, as long as a device s_j is within the coverage of a location c_i, $p(c_i, s_j) \geq P$; this can be achieved by setting $p_{\min}$ to a sufficiently large value.

Combining these together, we get the following special case of the decision version of the SP^3 problem: Given a candidate location set $\mathcal{C}$ of size k, and a device set $\mathcal{S}$ of size m, does there exist a charger placement $\mathcal{R}$ of size $\lfloor \frac{B}{p_{\min}} \rfloor$, such that $Q(\mathcal{R}, (1, 1, \ldots, 1)) \geq mP$?

It is not hard to see that the construction can be finished in polynomial time; thus, we reduce solving the NP-complete SC problem to solving a special case of the SP^3 problem, implying that SP^3 is NP-hard. It is easy to verify that SP^3 is in NP; the theorem follows immediately. □

4 Solution

4.1 Sketch

It is nontrivial to directly find an efficient algorithm for SP^3. Therefore, we first look at two special cases (SP^{3}fu and SP^{3}fn defined below) of SP^3 to reveal the problem structure and find key insights that help us design an efficient approximation, namely, TCA for SP^3.

SP^{3}fu. In this case, we assume that every charger can only work at a fixed power level and all chargers have the same power level. In other words, $h_1 = h_2 = \ldots = h_N = h$, and $p_1 = p_2 = \ldots = p_N = h \cdot p_{\min}$. Hence, we only need to determine charger placement and do not need to determine power allocation: the objective function $Q(\mathcal{R}, \mathbf{H})$ degenerates into $Q(\mathcal{R})$. For convenience, denote the power of each charger by p in SP^{3}fu. Formally,

Problem 2 (SP^3 with fixed and uniform power levels, SP^{3}fu). *Given a set $\mathcal{C}$ of candidate locations, a set $\mathcal{S}$ of devices, a power budget B, and a fixed power p, SP^3 is to find a charger placement $\mathcal{R}$ to maximize $Q(\mathcal{R})$, subject to the budget constraint, i.e., $|\mathcal{R}| \leq \lfloor \frac{B}{p} \rfloor$.*

For SP^{3}fu, we design an approximation algorithm shown in Algorithm 1 based on the good properties of $Q(\mathcal{R})$.

SP^{3}fn. In this case, we assume that every charger can only work at a fixed power level, but different chargers work at different power levels. Similarly, we have

Problem 3 (SP^3 with fixed and non-uniform power levels, SP^{3}fn). *Given a set $\mathcal{C}$ of candidate locations, a set $\mathcal{S}$ of devices, a power budget B, and a fixed power level h_i for each location c_i, SP^3 is to find a charger placement $\mathcal{R}$ to maximize $Q(\mathcal{R})$, subject to the budget constraint, i.e., $\sum_{c_i \in \mathcal{R}} p_i \leq B$.*

For SP^{3}fn, we design an approximation algorithm shown in Algorithm 2 based on the insights acquired from solving the first special case SP^{3}fu.

1. If the sensor is equipped with a battery of capacity w, for simplicity, we can define the average energy consumption rate as $P = \frac{p_a \cdot T_a + p_s \cdot (T - T_a) + w}{T}$. In this case, if the total power received by the sensor is larger than P, the over-received energy is also useless.

Finally, we design TCA for SP^3 based on the insights acquired from solving the second special case SP^{3}fn.

4.2 Details

4.2.1 Solving SP^{3}fu

To solve SP^{3}fu, we first prove that the objective function $Q(\mathcal{R})$ of SP^{3}fu has three tractable properties: nonnegativity, monotonicity, and submodularity, which enable us to propose a $(1-1/e)$-approximation algorithm.

Definition 2 (Nonnegativity, Monotonicity, and Submodularity). *Given a non-empty finite set $\mathcal{U}$, and a function f defined on the power set $2^{\mathcal{U}}$ of $\mathcal{U}$ with real values, f is called* nonnegative *if*

$$f(\mathcal{A}) \geq 0, \forall \mathcal{A} \subseteq \mathcal{U};$$

f is called monotone *if*

$$f(\mathcal{A}) \leq f(\mathcal{A}'), \forall \mathcal{A} \subseteq \mathcal{A}' \subseteq \mathcal{U};$$

f is called submodular *if*

$$f(\mathcal{A} \cup \{e\}) - f(\mathcal{A}) \geq f(\mathcal{A}' \cup \{e\}) - f(\mathcal{A}'), \forall \mathcal{A} \subseteq \mathcal{A}' \subseteq \mathcal{U}.$$

We have the following theorem:

Theorem 2. *$Q(\mathcal{R})$ in SP^{3}fu is nonnegative, monotone, and submodular.*

Proof. $Q(\mathcal{R})$ is nonnegative according to Definition 1. For all $\mathcal{R} \subseteq \mathcal{R}' \subseteq \mathcal{C}$, we have

$$Q(\mathcal{R}) = \sum_{j=1}^{M} Q_{\mathcal{R}}(s_j) \leq \sum_{j=1}^{M} Q_{\mathcal{R}'}(s_j) = Q(\mathcal{R}'),$$

implying that, $Q(\mathcal{R})$ is monotone. For all $\mathcal{R} \subseteq \mathcal{R}' \subseteq \mathcal{C}$, we need to prove

$$Q(\mathcal{R} \cup \{c\}) - Q(\mathcal{R}) \geq Q(\mathcal{R}' \cup \{c\}) - Q(\mathcal{R}').$$

It is sufficient to show that for any $s_j \in \mathcal{S}$, we have

$$Q_{(\mathcal{R}\cup\{c\})}(s_j) - Q_{\mathcal{R}}(s_j) \geq Q_{(\mathcal{R}'\cup\{c\})}(s_j) - Q_{\mathcal{R}'}(s_j).$$

Based on Eqs. (5) and (6), we prove the above inequality in three non-overlapping cases:

- $P_j \leq p_{\mathcal{R}}(s_j)$: since $p_{\mathcal{R}'}(s_j) \geq p_{\mathcal{R}}(s_j)$, we have

$$Q_{(\mathcal{R}\cup\{c\})}(s_j) - Q_{\mathcal{R}}(s_j) = 0 = Q_{(\mathcal{R}'\cup\{c\})}(s_j) - Q_{\mathcal{R}'}(s_j).$$

- $p_{\mathcal{R}}(s_j) < P_j < p_{\mathcal{R}'}(s_j)$: in this case, $Q_{(\mathcal{R}'\cup\{c\})}(s_j) - Q_{\mathcal{R}'}(s_j) = 0$, and we have

$$\begin{aligned} &Q_{(\mathcal{R}\cup\{c\})}(s_j) - Q_{\mathcal{R}}(s_j) \\ &\quad = \min\{P_j - p_{\mathcal{R}}(s_j), p_{(\mathcal{R}\cup\{c\})}(s_j) - p_{\mathcal{R}}(s_j)\} \\ &\quad = \min\{P_j - p_{\mathcal{R}}(s_j), p(c, s_j)\} \\ &\quad \geq 0 = Q_{(\mathcal{R}'\cup\{c\})}(s_j) - Q_{\mathcal{R}'}(s_j). \end{aligned}$$

- $p_{\mathcal{R}'}(s_j) \leq P_j$: in this case, we have

$$Q_{(\mathcal{R}\cup\{c\})}(s_j) - Q_{\mathcal{R}}(s_j) = \min\{P_j - p_{\mathcal{R}}(s_j), p(c, s_j)\},$$
$$Q_{(\mathcal{R}'\cup\{c\})}(s_j) - Q_{\mathcal{R}'}(s_j) = \min\{P_j - p_{\mathcal{R}'}(s_j), p(c, s_j)\}.$$

If $p(c, s_j) \leq P_j - p_{\mathcal{R}'}(s_j)$, then

$$Q_{(\mathcal{R}\cup\{c\})}(s_j) - Q_{\mathcal{R}}(s_j) = p(c, s_j) = Q_{(\mathcal{R}'\cup\{c\})}(s_j) - Q_{\mathcal{R}'}(s_j).$$

If $P_j - p_{\mathcal{R}'}(s_j) < p(c, s_j) < P_j - p_{\mathcal{R}}(s_j)$, then

$$\begin{aligned} &Q_{(\mathcal{R}\cup\{c\})}(s_j) - Q_{\mathcal{R}}(s_j) = p(c, s_j) \\ &\quad > P_j - p_{\mathcal{R}'}(s_j) = Q_{(\mathcal{R}'\cup\{c\})}(s_j) - Q_{\mathcal{R}'}(s_j). \end{aligned}$$

If $P_j - p_{\mathcal{R}}(s_j) \leq p(c, s_j)$, then

$$\begin{aligned} &Q_{(\mathcal{R}\cup\{c\})}(s_j) - Q_{\mathcal{R}}(s_j) = P_j - p_{\mathcal{R}}(s_j) \\ &\quad \geq P_j - p_{\mathcal{R}'}(s_j) = Q_{(\mathcal{R}'\cup\{c\})}(s_j) - Q_{\mathcal{R}'}(s_j). \end{aligned}$$

The theorem follows immediately. □

These properties enable us to propose an approximation algorithm of factor $(1-1/e)$ shown in Algorithm 1 [39], [40]. Since power levels are fixed in SP^{3}fu, we only have to determine the charger placement $\mathcal{R}$. In Algorithm 1, $\mathcal{R}$ is initialized to $\emptyset$; in each iteration, we add the location that maximizes the marginal gain of the objective function into $\mathcal{R}$. Here, the marginal gain means the additional charging quality from selecting an additional location, i.e., in each iteration, we select the location $c \in \mathcal{C} \setminus \mathcal{R}$ that maximize the following formula:

$$Q(\mathcal{R} \cup \{c\}) - Q(\mathcal{R}). \tag{7}$$

There are at most N iterations in Algorithm 1; in each iteration, we need to check at most N locations to find the location that maximizes the marginal gain. It takes $O(MN)$ time to compute $Q(\mathcal{R})$, thus, the time complexity of Algorithm 1 is $O(MN^3)$.

Algorithm 1. Greedy Algorithm (GA) for SP^{3}fu

Input: $\mathcal{C}$, $\mathcal{S}$, B, and the uniform power level p
Output: $\mathcal{R}$
1: $\mathcal{R} \leftarrow \emptyset$
2: **while** $|\mathcal{R}| < \lfloor \frac{B}{p} \rfloor$ **do**
3: select $c \in \mathcal{C} \setminus \mathcal{R}$ that maximizes $Q(\mathcal{R} \cup \{c\}) - Q(\mathcal{R})$
4: $\mathcal{R} \leftarrow \mathcal{R} \cup \{c\}$
5: **end while**
6: **return** $\mathcal{R}$

4.2.2 Solving SP^{3}fn

We now study the case where the power levels of chargers are *fixed but not necessarily the same*. To solve SP^{3}fn, an intuitive method is to use the same greedy idea as in Algorithm 1. However, we show in Fig. 2a that, this method may perform very poorly. In Fig. 2a, there are $N = L + 1$ candidate locations and $M = L + 1$ devices; $h_1 = h_2 = \cdots = h_{N-1} = 1$, and $h_N = L$; the radii of dashed circles indicate the maximum coverage distance of each charger; $p(c_1, s_1) = p(c_2, s_2) = \ldots = p(c_{N-1}, s_{N-1}) = p(c_N, s_N) - \epsilon$, where ϵ satisfies $0 < \epsilon < p(c_N, s_N)$. Given a power budget $B = L \cdot p_{\min}$, using Eq. (7), as c_N leads to the maximum marginal gain, c_N would be picked and achieves a charging quality of $p(c_1, s_1) + \epsilon$. However, the optimal solution that picks c_1, $c_2, \ldots,$ and c_{N-1} achieves a charging quality of $L \cdot p(c_1, s_1)$. When ϵ is approaching zero, this method could only achieve

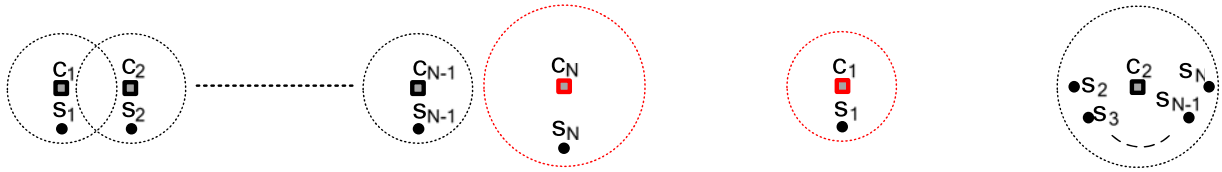

(a) With Eq. (7), charger c_N would be picked, while the optimal solution is to pick c_1, c_2,..., and c_{N-1}.

(b) With Eq. (8), charger c_1 would be picked; while the optimal solution is to pick c_2.

Fig. 2. Directly applying Eq. (7) or Eq. (8) to SP^{3}fn may result in a very poor performance.

approximately $1/L$ of the charging quality returned by the optimal solution.

Another intuitive method is that, as long as there is remaining power budget, in each iteration, we add the location $c_x \in \mathcal{C} \setminus \mathcal{R}$ that maximizes the ratio of the marginal gain to the power cost, i.e.,

$$c_x \leftarrow \underset{c_x \in \mathcal{C}\setminus\mathcal{R}, \sum_{c_i \in \mathcal{R}\cup\{c_x\}} p_i \le B}{\arg\max} \frac{Q(\mathcal{R}\cup\{c_x\}) - Q(\mathcal{R})}{p_x}. \quad (8)$$

However, we show in Fig. 2b that, this method may also perform poorly. In Fig. 2b, there are 2 candidate locations and $M = L+1$ devices; $h_1 = 1$, and $h_2 = L$; $p(c_1, s_1) = p(c_2, s_2) \cdots = p(c_2, s_{M-1}) = p(c_2, s_M) + \epsilon$, where ϵ satisfies $0 < \epsilon < p(c_1, s_1)$. Given a power budget $B = L \cdot p_{\min}$, using Eq. (8), the charger c_1 would be picked and achieves a charging quality of $p(c_1, s_1)$. However, the optimal solution that picks c_2 achieves a charging quality of $(L-1)\cdot p(c_1, s_1) + p(c_2, s_M)$. When ϵ is approaching zero, this method could only achieve approximately $1/L$ of the charging quality returned by the optimal solution.

However, if we simultaneously apply the above two methods to SP^{3}fn, and return the better one of the two results [41], we would get an approximation algorithm, as shown in Algorithm 2, of factor $\frac{1}{2}(1-\frac{1}{e})$. It is not hard to see the time complexity of Algorithm 2 is also $O(MN^3)$.

Algorithm 2. Approx. Algorithm (AA) for SP^{3}fn

Input: $\mathcal{C}$, $\mathcal{S}$, B, and the power levels $h_1, h_2, \ldots, h_N$
Output: $\mathcal{R}$

$\mathcal{R}_1 \leftarrow \emptyset, \mathcal{R}_2 \leftarrow \emptyset$
while $B \ge \sum_{c_i \in \mathcal{R}_1} p_i + \min_{c_i \in \mathcal{C}\setminus\mathcal{R}_1} p_i$ **do**
  select $c \in \mathcal{C} \setminus \mathcal{R}_1$ that maximizes $Q(\mathcal{R}_1 \cup \{c\}) - Q(\mathcal{R}_1)$, subject to $\sum_{c_i \in \mathcal{R}_1 \cup \{c\}} p_i \le B$
  $\mathcal{R}_1 \leftarrow \mathcal{R}_1 \cup \{c\}$
end while
while $B \ge \sum_{c_i \in \mathcal{R}_2} p_i + \min_{c_i \in \mathcal{C}\setminus\mathcal{R}_2} p_i$ **do**
  select $c_x \in \mathcal{C} \setminus \mathcal{R}_2$ that maximizes $\frac{Q(\mathcal{R}_2\cup\{c_x\}) - Q(\mathcal{R}_2)}{p_x}$ subject to $\sum_{c_i \in \mathcal{R}_2 \cup \{c_x\}} p_i \le B$
  $\mathcal{R}_2 \leftarrow \mathcal{R}_2 \cup \{c_x\}$
end while
return $\arg\max_{\mathcal{R}' \in \{\mathcal{R}_1, \mathcal{R}_2\}} Q(\mathcal{R})$

4.2.3 Solving SP^3

In this section, we present an approximation algorithm, i.e., TCA in Algorithm 3 for the general SP^3 problem.

Before formally explaining TCA, we first consider the following variant of SP^3, where we can *place multiple chargers at one location*:

Problem 4 (VSP^3). *For each candidate location c_i, we are given L chargers with* exactly *different power levels, i.e., the power levels of these chargers are $1, 2, \ldots,$ and L. We use (c_i, h_k) to denote the charger of a constant power level h_k that can only be placed at c_i. Note that there are, in total, $N \cdot L$ chargers. Given a power budget B, how do we find a charger placement that maximizes the objective function defined below?*

Algorithm 3. Two-Choice-Based Alg. (TCA) for SP^3

Input: $\mathcal{C}$, $\mathcal{S}$, and B
Output: $\mathcal{R}$ and $\mathbf{H}$

$\mathcal{Z} \leftarrow \mathcal{C} \times \mathcal{H}$ //the Cartesian product
$\mathcal{Z}_1 \leftarrow \emptyset, \mathbf{H}_1 \leftarrow \mathbf{0}$
while $B \ge \min_{(c_i,h_k)\in\mathcal{Z}\setminus\mathcal{Z}_1} p(h_k) + \sum_{(c_i,h_k)\in\mathcal{Z}_1} p(h_k)$ **do**
  select $(c,h) \in \mathcal{Z} \setminus \mathcal{Z}_1$ that maximizes $Q(\mathcal{Z}_1 \cup \{(c,h)\}) - Q(\mathcal{Z}_1)$ subject to $\sum_{(c_i,h_k)\in\mathcal{Z}_1\cup\{(c,h)\}} p(h_k) \le B$
  $\mathcal{Z}_1 \leftarrow \mathcal{Z}_1 \cup \{(c,h)\}$
  if $\mathbf{H}_1[c] < h$ **then** $\mathbf{H}_1[c] \leftarrow h$
end while
$(\mathcal{R}_1, \mathbf{H}_1) \leftarrow$ RDU $(\mathcal{C}, \mathcal{S}, B, \mathbf{H}_1)$
$\mathcal{Z}_2 \leftarrow \emptyset, \mathbf{H}_2 \leftarrow \mathbf{0}$
while $B \ge \min_{(c_i,h_k)\in\mathcal{Z}\setminus\mathcal{Z}_2} p(h_k) + \sum_{(c_i,h_k)\in\mathcal{Z}_2} p(h_k)$ **do**
  select $(c,h) \in \mathcal{Z} \setminus \mathcal{Z}_2$ that maximizes $\frac{Q(\mathcal{Z}_2\cup\{(c,h)\}) - Q(\mathcal{Z}_2)}{p(h)}$ subject to $\sum_{(c_i,h_k)\in\mathcal{Z}_2\cup\{(c,h)\}} p(h_k) \le B$
  $\mathcal{Z}_2 \leftarrow \mathcal{Z}_2 \cup \{(c,h)\}$
  if $\mathbf{H}_2[c] < h$ **then** $\mathbf{H}_2[c] \leftarrow h$
end while
$(\mathcal{R}_2, \mathbf{H}_2) \leftarrow$ RDU $(\mathcal{C}, \mathcal{S}, B, \mathbf{H}_2)$
return $\arg\max_{(\mathcal{R},\mathbf{H})\in\{(\mathcal{R}_1,\mathbf{H}_1),(\mathcal{R}_2,\mathbf{H}_2)\}} Q(\mathcal{R}, \mathbf{H})$

Denote the set $\{1, 2, \ldots, L\}$ by $\mathcal{H}$; denote by $\mathbf{I}_i$ a row vector where the ith element is 1 and all of the other elements are zeros, i.e., $\mathbf{I}_i = (0, 0, \ldots, 1, \ldots, 0)$. We use $\mathbf{H}[c_i]$ to represent the power level of location c_i.

Let $\mathcal{Z}$ be the Cartesian product of $\mathcal{C}$ and $\mathcal{H}$; denote by $\mathcal{Z}'$ a subset of $\mathcal{Z}$. We redefine several functions for VSP^3 via overloading. The power $p(c_i, s_j, h_k)$ received by device s_j from c_i (its power level is h_k) is

$$p(c_i, s_j, h_k) = \begin{cases} \frac{\alpha \cdot h_k \cdot p_{min}}{(d(c_i,s_j)+\beta)^2}) & d(c_i, s_j) \le D(h_k), \\ 0 & d(c_i, s_j) > D(h_k). \end{cases} \quad (9)$$

Given a charger placement $\mathcal{Z}'$, the total power $p_{\mathcal{Z}'}(s_j)$ received by device s_j is $p_{\mathcal{Z}'}(s_j) = \sum_{(c_i,h_k)\in\mathcal{Z}'} p(c_i, s_j, h_k)$. The charging quality of $\mathcal{Z}'$ on s_j is

$$Q_{\mathcal{Z}'}(s_j) = \min\{p_{\mathcal{Z}'}(s_j), P_j\}. \quad (10)$$

The objective function is $Q(\mathcal{Z}') = \sum_{j=1}^{M} Q_{\mathcal{Z}'}(s_j)$.

The main idea of TCA is as follows. We first use the two greedy heuristics (i.e., Eqs. (7) and (8)) to solve VSP^3, and get two results $\mathcal{Z}_1$ and $\mathcal{Z}_2$, respectively. We then invoke the RDU sub-procedure to transform $\mathcal{Z}_1$ and $\mathcal{Z}_2$ into $(\mathcal{R}_1, \mathbf{H}_1)$ and $(\mathcal{R}_2, \mathbf{H}_2)$, respectively. We choose the better one of them as the final solution to SP^3.

The RDU sub-procedure (Algorithm 4) works as follows (take $\mathcal{Z}_1$ for example): *Note that there may be more than one charger placed at a candidate location in $\mathcal{Z}_1$, we thus retain only one charger for each location in transforming $\mathcal{Z}_1$ into $\mathcal{R}_1$ and $\mathbf{H}_1$, which implies that there may be some unused budget for $\mathcal{R}_1$ and $\mathbf{H}_1$.* For each location c_i, we set $\mathbf{H}_1[c_i]$ to be the maximum value of h_k among all $(c_i, h_k) \in \mathcal{Z}_1$, i.e., $\mathbf{H}_1[c_i] = \max_{(c_i,h_k)\in\mathcal{Z}_1} h_k$ (line 6 of Algorithm 3). For each location c_i, if $\mathbf{H}_1[c_i] > 0$, we add it into $\mathcal{R}_1$, which is equivalent to $\mathcal{R}_1 = \{c_i | (c_i, h_k) \in \mathcal{Z}_1\}$ (lines 2-4 of Algorithm 4). In the following, we try to improve $\mathcal{R}_1$ and $\mathbf{H}_1$ by utilizing the remaining budget $(B - B'_1)$ (lines 5-8 of Algorithm 4). In each iteration, we allocate a fixed power $p_{\min}$ to the location that maximizes the marginal objective gain,[2] that is, we increase the power level of location c_i by 1, if its power level is less than L and it maximizes $Q(\mathcal{R} \cup \{c_i\}, \mathbf{H} + \mathbf{I}_i) - Q(\mathcal{R}, \mathbf{H})$.

Time Complexity. There are at most NL iterations in each while-loop of Algorithm 3; in each iteration, at most NL pairs of c and h are checked, and computing $Q(\mathcal{Z})$ needs $O(MNL)$ time. Therefore, each while-loop takes $O(MN^3L^3)$ time. For Algorithm 4, lines 2-4 takes $O(N)$ time; there are $B - B'$ iterations in the while-loop; in each iteration, at most N locations are checked, and each check takes $O(MN)$ time. Therefore, the time complexity of Algorithm 4 is $O(N + (B - B')MN^2)$. Observing $B - B' < NL/2$, we have $O(N + (B - B')MN^2) = O(MN^3L)$. In summary, the time complexity of TCA is $O(MN^3L^3)$.

Algorithm 4. Remove Duplication and Utilize (RDU)

Input: $\mathcal{C}$, $\mathcal{S}$, B, and $\mathbf{H}$
Output: $\mathcal{R}$ and $\mathbf{H}$
1: $\mathcal{R} \leftarrow \emptyset$, $B' \leftarrow 0$
2: **for all** $\mathbf{H}[c_i] > 0$ **do**
3: $\quad \mathcal{R} \leftarrow \mathcal{R} \cup \{c_i\}$, $B' \leftarrow B' + p(\mathbf{H}[c_i])$
4: **end for**
5: **while** $B - B' \geq p_{\min}$ **do**
6: $\quad$ select c_i that maximizes $Q(\mathcal{R} \cup \{c_i\}, \mathbf{H} + \mathbf{I}_i) - Q(\mathcal{R}, \mathbf{H})$ subject to $\mathbf{H}[c_i] + 1 \leq L$
7: $\quad \mathcal{R} \leftarrow \mathcal{R} \cup \{c_i\}$, $\mathbf{H}[c_i] \leftarrow \mathbf{H}[c_i] + 1$, $B' \leftarrow B' + p_{\min}$
8: **end while**
9: **return** $(\mathcal{R}, \mathbf{H})$

Approximation Ratio. Theorem 3 gives the performance guarantee of TCA. Later, we will see in the simulations that, the gap between TCA and the optimal solution is and 2.0 percent on average, and 4.5 percent at most.

Theorem 3. *TCA is a factor $\frac{1-1/e}{2L}$ approximation algorithm for SP^3.*

2. We can further improve lines 5-8 of Algorithm 4 by applying both Eqs. (7) and (8), and choosing the better one. However, the improvement would be little. We choose the current form for brevity.

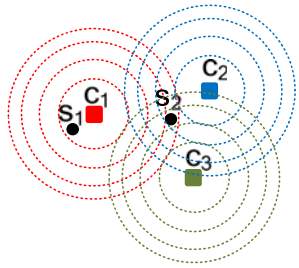

Fig. 3. There are three candidate locations and two devices. The radii of dashed circles show the maximum cover distances of four different power levels.

Proof. Denote by $(\mathcal{R}^*, \mathbf{H}^*)$ the optimal solution to SP^3, and by $(\mathcal{R}, \mathbf{H})$ the solution returned by TCA. We want to prove that,

$$\frac{Q(\mathcal{R}, \mathbf{H})}{Q(\mathcal{R}^*, \mathbf{H}^*)} \geq \frac{1 - 1/e}{2L}.$$

Let $\mathcal{Z}^*$ be the optimal solution to VSP^3, and let

$$\mathcal{Z}' = \arg\max_{\mathcal{Z}' \in \{\mathcal{Z}_1, \mathcal{Z}_2\}} Q(\mathcal{Z}')$$

where $\mathcal{Z}_1$ and $\mathcal{Z}_2$ are the solutions generated by lines 3-7 and 9-14 of TCA, respectively. According to the results in Section 4.2.2, we know

$$Q(\mathcal{Z}') \geq (1 - 1/e)/2Q(\mathcal{Z}^*).$$

Notice that, if we restrict the number of chargers that can be placed at each candidate location to one, the VSP^3 problem is equivalent to SP^3, i.e., SP^3 is a special case of VSP^3. From this viewpoint, we have

$$Q(\mathcal{Z}^*) \geq Q(\mathcal{C}^*, \mathbf{H}^*).$$

In $\mathcal{Z}_1$ (resp. $\mathcal{Z}_2$), we can place at most L chargers at one location. When transforming $\mathcal{Z}_1$ (resp. $\mathcal{Z}_2$) into $\mathcal{R}_1$ and $\mathbf{H}_1$ (resp. $\mathcal{R}_2$ and $\mathbf{H}_2$), for each location, we retain the charger that has the largest power level, if any. Therefore, we have

$$Q(\mathcal{R}_1, \mathbf{H}_1) \geq Q(\mathcal{Z}_1)/L, \quad \text{and} \quad Q(\mathcal{R}_2, \mathbf{H}_2) \geq Q(\mathcal{Z}_2)/L.$$

Combining them together, we have

$$\begin{aligned} Q(\mathcal{R}, \mathbf{H}) &= \max\{Q(\mathcal{R}_1, \mathbf{H}_1), Q(\mathcal{R}_2, \mathbf{H}_2)\} \\ &\geq \frac{\max\{Q(\mathcal{Z}_1), Q(\mathcal{Z}_2)\}}{L} = \frac{Q(\mathcal{Z}')}{L} \\ &\geq \frac{1 - 1/e}{2L} Q(\mathcal{Z}^*) \geq \frac{1 - 1/e}{2L} Q(\mathcal{R}^*, \mathbf{H}^*). \end{aligned}$$

The theorem follows immediately. □

4.3 Example of Running TCA

We use the example shown in Fig. 3 to explain how TCA works. There are 3 candidate locations and 2 devices. Following existing works [15], [17], [18], we assume that, $p_{\min} = 50$, $L = 4$, $p_{th} = 0.01$, $\alpha = 0.64$, and $\beta = 30$. Given these parameters, we have $D(1) \approx 27$, $D(2) = 50$, $D(3) \approx 68$, and $D(4) \approx 83$. The radii of dashed circles show the maximum cover distances of four different power levels. We can compute that, $d(c_1, s_1) = 20$, $d(c_1, s_2) = 70$, $d(c_2, s_2) = 40$, and $d(c_3, s_2) = 60$. The average power consumption rate of

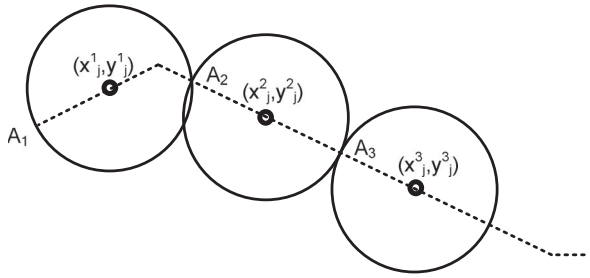

Fig. 4. The trajectory of device s_j is represented by a series of tuples. The kth tuple (x_j^k, y_j^k, t_j^k) indicates that, s_j stays within the circle, whose center and radius are (x_j^k, y_j^k) and E, respectively, for a time duration of t_j^k.

s_1 or s_2 is 0.07, i.e., $P_1 = P_2 = 0.07$. Given a power budget $B = 500$, we now check how TCA works.

In lines 2-7 of Algorithm 3, we first check which (c, h) gives the maximal marginal objective gain. For c_1, we have $Q(\{(c_1, 1)\}) = 0.0128$, $Q(\{(c_1, 2)\}) = 0.0256$, $Q(\{(c_1, 3)\}) = 0.0384$, and $Q(\{(c_1, 4)\}) = 0.064$; for c_2 and c_3, we can compute these values in a similar way. Thus, in the first iteration of lines 2-8, we add $(c_1, 4)$ into $\mathcal{Z}_1$. It is worth noting that, in the second iteration, $Q(\{(c_1, 4)\} \cup \{(c_1, 2)\}) - Q(\{(c_1, 4)\}) = \min\{p(c_1, s_1, 2), P_1 - p(c_1, s_1, 4)\} = 0.0188$ (see Eqs. (9) and (10)). The reader can check that, $\mathcal{Z}_1$ would be $\{(c_1, 4), (c_2, 4), (c_1, 2)\}$.

Note that, for each location, we retain only one charger which has the largest power level in $\mathcal{Z}_1$. Then we get $\mathcal{R}_1 = \{c_1, c_2\}$ and $\mathbf{H}_1 = (4, 4, 0)$. In lines 5-8 of Algorithm 4, we try to utilize the remaining budget $500 - (4 + 4) \times 50 = 100$. We find that, the distance between c_3 and s_2 is larger than $D(2)$, thus, there is no need to allocate the remaining 100 units of power to c_3. Finally we have $\mathcal{R}_1 = \{c_1, c_2\}$ and $\mathbf{H}_1 = (4, 4, 0)$.

Similarly, after running lines 9-14, we would have $\mathcal{Z}_2 = \{(c_1, 4), (c_1, 1), (c_2, 2), (c_2, 3)\}$. Through removing duplications, we have $\mathcal{R}_2 = \{c_1, c_2\}$ and $\mathbf{H}_2 = (4, 3, 0)$. After utilizing the remaining budget, we also have $\mathcal{R}_2 = \{c_1, c_2\}$ and $\mathbf{H}_2 = (4, 4, 0)$.

The final solution is $\mathcal{R} = \{c_1, c_2\}$ and $\mathbf{H} = (4, 4, 0)$, yielding an objective of $Q(\mathcal{R}, \mathbf{H}) = 0.0902$.

5 Extensions

In this section, we provide three extensions of SP^3. The first is to deal with *mobile* devices instead of stationary devices (Section 5.1). The second is to study the reconfiguration problem when devices leave and enter the target area over time (Section 5.2). And the last is to optimize charging quality with more candidate locations (Section 5.3).

5.1 Mobile Rechargeable Devices

In SP^3, we assume that rechargeable devices are stationary. However, it is more realistic to consider mobile rechargeable devices. We consider MP^3 problem in this section where 'M' denotes mobile.

In Fig. 4, the trajectory of a device s_j is shown in dashed lines. Theoretically, we can compute the integral over its trajectory to obtain the charging quality given a charger placement and power allocation. However, this is too complicated. Instead, we resort to discrete time modeling.

Denote by E the circle radius in the figure, and obviously, E can be used to control modeling precision. The trajectory of s_j is represented by a set of tuples, i.e., (x_j^k, y_j^k, t_j^k). The kth tuple (x_j^k, y_j^k, t_j^k) means that, s_j stays with the circle, whose center and radius are (x_j^k, y_j^k) and E, respectively, for a time duration of t_j^k.

We now show how to obtain these tuples. Denote by A_1 the starting point of the trajectory. The distance between A_1 and (x_j^1, y_j^1) is E, thus, we have the first circle. Denote by A_2 the intersection point of the trajectory and the first circle. The distance between A_2 and (x_j^2, y_j^2) is also E, thus, we have the second circle; and so on. t_j^k is set to be the time duration when s_j is with its kth circle.

Given a placement $\mathcal{R}$ and an allocation $\mathbf{H}$, the total power $p_{\mathcal{R},\mathbf{H}}(s_j, t_j^k)$ received by a device s_j at its kth position is denoted by

$$p_{\mathcal{R},\mathbf{H}}(s_j, t_j^k) = \sum_{c_i \in \mathcal{R}} p(c_i, s_j). \tag{11}$$

Similarly, the charging quality of $\mathcal{R}$ and $\mathbf{H}$ on s_j at its kth position is denoted by

$$Q_{\mathcal{R},\mathbf{H}}(s_j, t_j^k) = \min\{p_{\mathcal{R},\mathbf{H}}(s_j, t_j^k), P_j\}. \tag{12}$$

And the charging quality of $\mathcal{R}$ and $\mathbf{H}$ on s_j is defined as the *weighted* sum of $Q_{\mathcal{R},\mathbf{H}}(s_j, t_j^k)$, i.e.,

$$Q_{\mathcal{R},\mathbf{H}}(s_j) = \frac{1}{\sum_{i=1}^{K} t_j^i} \sum_{k=1}^{K} t_j^k Q_{\mathcal{R},\mathbf{H}}(s_j, t_j^k). \tag{13}$$

With the above discrete time-based modeling, we can formulate a problem similar to SP^3. Fortunately, MP^3 also has the aforementioned tractable properties as SP^3, based on which we can tailor Algorithm 3 to MP^3 and yield an approximation algorithm of the same factor as TCA. Note that, the discrete time model could be arbitrarily precise when E is sufficiently small.

5.2 Reconfiguration

Mobile devices may leave or enter the target area over time, which makes the current charger placement and power allocation not optimal in terms of charging quality. Hence, we may need to switch from one charger placement and power allocation to another one.

First, when should we reconfigure the charger placement and power allocation? It is reasonable to start a reconfiguration only when a certain percent of devices leave or enter the target area. For example, when $\mathcal{S}$ changes into $\mathcal{S}'$, if $\frac{|\mathcal{S}' \bigcup \mathcal{S} - \mathcal{S}' \bigcap \mathcal{S}|}{|\mathcal{S}|} \geq \delta$, we start a reconfiguration. Here, δ represents the percentage threshold.

Second, how should we maintain smoothness when switching one solution to another one? By 'smoothness' we mean that, the received power by a device should not decrease or increase too much when we change one charger placement and power allocation into another one. Taking Fig. 3 for example, suppose the power budget B is $6 \cdot p_{min}$ and the current power allocation $\mathbf{H}$ is $(4, 2, 0)$. Now a new device s_3 emerges and it is within $D(2)$ distance from c_3 and within $D(3)$ distance from c_2. We have two new power

allocations: $\mathbf{H}_1 = (2, 2, 2)$ and $\mathbf{H}_2 = (3, 3, 0)$. Although both of them satisfy the budget constraint, the latter one is better from the perspective from smoothness. For s_1, $p_{\mathbf{H}}(s_1) = \frac{\alpha \cdot 4 \cdot p_{\min}}{(d(c_1,s_1)+\beta)^2}$, $p_{\mathbf{H}_1}(s_1) = \frac{\alpha \cdot 2 \cdot p_{\min}}{(d(c_1,s_1)+\beta)^2}$, and $p_{\mathbf{H}_2}(s_1) = \frac{\alpha \cdot 3 \cdot p_{\min}}{(d(c_1,s_1)+\beta)^2}$. For s_2, $p_{\mathbf{H}}(s_2) = \frac{\alpha \cdot 4 \cdot p_{\min}}{(d(c_1,s_2)+\beta)^2} + \frac{\alpha \cdot 2 \cdot p_{\min}}{(d(c_2,s_2)+\beta)^2}$, $p_{\mathbf{H}_1}(s_2) = \frac{\alpha \cdot 2 \cdot p_{\min}}{(d(c_2,s_2)+\beta)^2}$, and $p_{\mathbf{H}_2}(s_2) = \frac{\alpha \cdot 3 \cdot p_{\min}}{(d(c_2,s_2)+\beta)^2}$. We see that, for either s_1 or s_2, the received power fluctuates less when switching from $\mathbf{H}$ to $\mathbf{H}_2$ than $\mathbf{H}_1$. Based on this observation, without loss of generality, the reconfiguration cost from $(\mathcal{R}, \mathbf{H})$ to $(\mathcal{R}', \mathbf{H}')$ can be defined as

$$f(\mathbf{H}, \mathbf{H}') = \sum_{i=1}^{N} |h_i - h_i'|. \tag{14}$$

To keep smoothness, the reconfiguration cost should not exceed a threshold, denoted by F. More formally,

Problem 5 (Cost-constrained Reconfiguration Problem, CRP). *Given current device set $\mathcal{S}$, charger placement $\mathcal{R}$, and power allocation $\mathbf{H}$, if $\mathcal{S}$ evolves into $\mathcal{S}'$, find a new charger placement $\mathcal{R}'$ and power allocation $\mathbf{H}'$ that maximize the charging quality, subject to $f(\mathbf{H}, \mathbf{H}') \leq F$.*

Formally, CRP can be formulated as follows:

$$\max \quad Q(\mathcal{R}', \mathbf{H}') \tag{15a}$$

$$\text{s.t.} \quad f(\mathbf{H}, \mathbf{H}') \leq F \tag{15b}$$

$$(\mathcal{R}, \mathbf{H}) = \text{TCA}(\mathcal{S}) \tag{15c}$$

$$\sum_{c_i \in \mathcal{R}'} p_i \leq B \tag{15d}$$

where Eq. (15c) means $\mathcal{R}$ and $\mathbf{H}$ are computed by TCA (i.e., Algorithm 3). It is not hard to see that CRP is also NP-complete, since SP^3 is a special case of CRP when F is sufficiently large. In the following, we design an approximation algorithm for CRP in Algorithm 5.

Algorithm 5. Iteratively Adjustment Alg. (IAA) for CRP

Input: $\mathcal{C}$, $\mathcal{S}$, B, $\mathcal{S}'$, and F
Output: $\mathcal{R}'$ and $\mathbf{H}'$
1: $(\mathcal{R}, \mathbf{H}) = \text{TCA}(\mathcal{S})$
2: $(\mathcal{R}_t, \mathbf{H}_t) = \text{TCA}(\mathcal{S}')$
3: $(\mathcal{R}', \mathbf{H}') \leftarrow (\mathcal{R}_t, \mathbf{H}_t)$
4: **while** $f(\mathbf{H}, \mathbf{H}') > F$ **do**
5: $\quad i \leftarrow \arg\min_{1 \leq i \leq N, h_i' > h_i} Q(\mathcal{R}', \mathbf{H}') - Q(\mathcal{R}', \mathbf{H}' - \mathbf{I}_i)$
6: $\quad \mathbf{H}' \leftarrow \mathbf{H}' - \mathbf{I}_i$
7: $\quad$ randomly select j such that $h_j > h_j'$
8: $\quad \mathbf{H}' \leftarrow \mathbf{H}' + \mathbf{I}_j$
9: **end while**
10: **return** $(\mathcal{R}', \mathbf{H}')$

The main idea of Algorithm 5 is as follows: we first employ TCA to compute two solutions for $\mathcal{S}$ and $\mathcal{S}'$, respectively (lines 1-2); then we iteratively adjust $(\mathcal{R}', \mathbf{H}')$ in order to make sure $f(\mathbf{H}, \mathbf{H}') \leq F$ (lines 4-9). In each iteration of the while-loop, we decrease the power level of c_i by one, which satisfies $1 \leq i \leq N$ and $h_i' > h_i$, to minimize the marginal quality loss, i.e., $Q(\mathcal{R}', \mathbf{H}') - Q(\mathcal{R}', \mathbf{H}' - \mathbf{I}_i)$; here, $h_i' > h_i$ ensures that decreasing h_i' does not increase $f(\mathbf{H}, \mathbf{H}')$; then we randomly select c_j that satisfies $h_j > h_j'$, and increase h_j' by one, which would definitely reduce $f(\mathbf{H}, \mathbf{H}')$.

Following similar analyses to that of Algorithm 3, we know the time complexity of Algorithm 5 is also $O(MN^3L^3)$. The following gives the performance guarantee of IAA.

Theorem 4. *IAA is a factor $\frac{(1-1/e)F}{4BL}$ approximation algorithm for CRP.*

Proof. Let us first compare the charging qualities of $(\mathcal{R}_t, \mathbf{H}_t)$ (line 2) and $(\mathcal{R}', \mathbf{H}')$ (line 10). Due to the submodularity of $Q(\mathcal{R}, \mathbf{H})$ and the way we decrease power levels (lines 5-6), we can guarantee that the charging quality loss due to power levels decrease is no more than $\frac{2B-F}{2B} Q(\mathcal{R}_t, \mathbf{H}_t)$. Hence, we have

$$Q(\mathcal{R}', \mathbf{H}') \geq \frac{F}{2B} Q(\mathcal{R}_t, \mathbf{H}_t).$$

According to Theorem 3, we have

$$Q(\mathcal{R}_t, \mathbf{H}_t) \geq \frac{1 - 1/e}{2L} OPT^*$$

where OPT^* denotes the optimal solution for the new device set $\mathcal{S}'$ irrespective of reconfiguration cost threshold, i.e., F. Obviously, we have $OPT^* \geq OPT$, where OPT denotes the optimal solution for the new device set $\mathcal{S}'$ with respect to F. Combining above formulas together, we have

$$Q(\mathcal{R}', \mathbf{H}') \geq \frac{(1 - 1/e)F}{4BL} OPT.$$

The theorem follows immediately. □

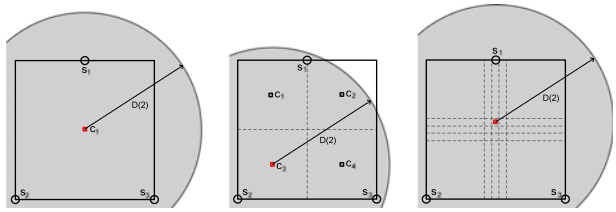

(a) $G = 1$ (b) $G = 2$ (c) $G = 19$

Fig. 5. Improving charging quality through more candidate locations. The grey circle indicates the final charger placement and power allocation for each G.

5.3 Optimization with More Candidate Locations

The candidate locations for placing wireless chargers are fixed in aforementioned problems. In this section, we remove this constraint and allow chargers to be placed at any location within the target area.

To cope with the infinitive candidate locations, we turn to the discrete space model: for $G = 1, 2, \ldots,$ we partition the target area into $G \times G$ grids and use these $G \times G$ grid centers as the candidate locations; the iteration stops when the gap between the charging quality in the Gth iteration and the best quality among previous $(G-1)$ iterations is no more than a threshold.

Fig. 5 shows an example. There are 3 devices in the plane (60×60). Following existing works [15], [17], [18], we assume that, $p_{\min} = 50$, $L = 2$, $p_{th} = 0.01$, $\alpha = 0.64$, and

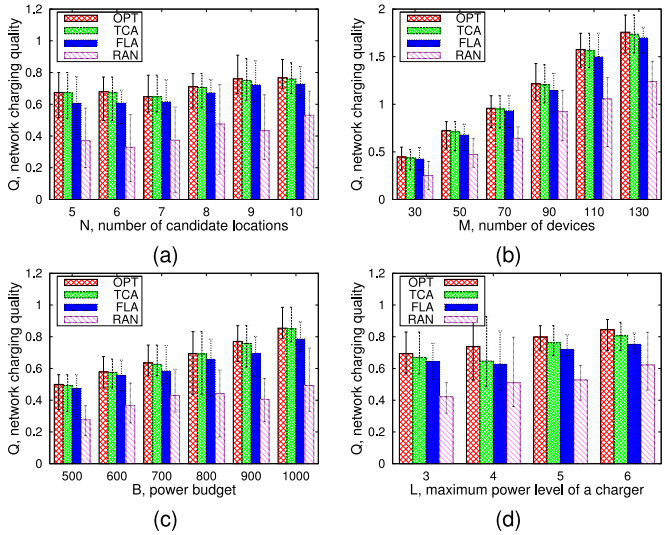

Fig. 6. Evaluation results on small instances of SP^3 (the default setting is $N = 8$, $M = 50$, $B = 800$, $L = 4$, and the side length of the 2-D plane is 300 m).

$\beta = 30$. Given these parameters, we have $D(1) \approx 27$ and $D(2) = 50$. The average power consumption rate of each device is 0.02, i.e., $P_1 = P_2 = P_3 = 0.02$. The grey circle indicates the coverage of a charger. Given a power budget $B = 100$, we now show how the placement and allocation evolves as G increases.

When $G = 1$ (Fig. 5a), the final placement is $\{c_1\}$ and the power allocation is $\mathbf{H} = (2)$, yielding a charging quality of 0.045. When $G = 2$ (Fig. 5b), the final placement is $\{c_3\}$ and the power allocation is $\mathbf{H} = (0, 0, 2, 0)$, yielding a charging quality of 0.031. When $G = 19$ (Fig. 5c), the final placement is $\{c_{162}\}$ and the power allocation is $\mathbf{H} = (0, 0, \ldots, 2, \ldots, 0)$, yielding a charging quality of 0.047, which is also the optimal solution of the example.

6 Performance Evaluation

In this section, we first introduce baseline algorithms (Section 6.1), then we present simulation results and key findings (Sections 6.2, 6.3, 6.4, and 6.5).

6.1 Baselines

We introduce three algorithms for comparison.

Random Algorithm (RAN): It should generate each possible solution with the same probability. We implement it as follows. Let $b = 0$ at the beginning. In the ith iteration, we uniformly generate a random integer x_i in the range $[1, L]$, let $b = b + x_i$; if $(B/p_{\min} - b)$ is no less than L, go to the next iteration, else let x_{i+1} be $(B/p_{\min} - b)$. Suppose the index of the last iteration is k, for $k + 1 \leq j \leq N$, we let x_j be 0. We then sort $x_1, x_2, \ldots, x_N$ randomly to get a random permutation $(x'_1, \ldots, x'_N)$. For each c_i, we set $\mathbf{H}[c_i] = x'_i$ in the random solution.

Fixed Level Algorithm (FLA): It consists of two phases. The first phase is to compute the optimal power level of each location irrespective of the other locations, i.e.,

$$h_i = \arg \max_{h_i \in \{1,\ldots,L\}} \frac{\sum_{j=1}^{M} Q_{\{c_i\}}(s_j)}{p(h_i)}. \quad (16)$$

The second phase is to invoke Algorithm 2 to generate a charger placement.

Optimal Algorithm (OPT): All of SP^3, MP^3, and CRP are NP-complete. We simply use brute force to find the optimal solution. Due to its high time complexity $O(ML^N)$, it is only practical for small instances.

6.2 Results of SP^3

6.2.1 Setup

We evaluate the performance of TCA on SP^3 instances in this section. We assume that wireless devices and candidate locations are randomly distributed over a $1{,}000\ \mathrm{m} \times 1{,}000\ \mathrm{m}$ two-dimensional square area. The default number of candidate locations is 20. The minimum power $p_{\min}$ of a charger is 50. By default, the maximum power level L is 6. The default number of devices is 200. Following prior works [15], [17], we set $\alpha = 0.64$ and $\beta = 30$ in the charging model (Eq. (3)). The threshold p_{th} of negligible power is 0.01. Therefore, the minimum coverage radius is $D(1) = \sqrt{0.64 \times 50/0.01} - 30 \approx 27\ \mathrm{m}$ (see Eq. (4)), and by default the maximum coverage radius is $D(6) = \sqrt{0.64 \times 300/0.01} - 30 \approx 109\ \mathrm{m}$. The average power consumption rate of each device is uniformly generated between 0.02 and 0.03. The default power budget is 3,000.

6.2.2 Results

As we have mentioned, it is impractical to run OPT using brute force in general; we thus use the following setting to generate some small instances for comparing TCA with OPT: $N = 8$, $M = 50$, $B = 800$, $L = 4$, and the side length of the 2-D plane is 300 m. Fig. 6 shows the results of different experiment setups of small instances. We ran each different setup ten times and averaged the results. The max and min values among ten runs are also provided in the figures.

In general, TCA achieves a near optimal solution and outperforms the other algorithms. Specifically, *the gap between TCA and OPT is 4.5 percent at most and 2.0 percent on average*. This observation validates our theoretical results. FLA uses a similar idea as our algorithm, thus, it performs much better than RAN, which has the worst performance of all the setups. On average, the charging quality RAN achieves is roughly 64.4 percent of that of TCA.

In Figs. 6a and 6d, when the number of candidate locations increases or the maximum power level of a candidate location increases, the chance of having a better solution goes up, so the overall charging quality increases. Since a charger can transfer power to multiple devices simultaneously [30], when the number of energy receiving devices increases, the total power received by all devices would be larger than before, so the charging quality increases as well. This is what we noticed in Fig. 6b. Fig. 6c presents the performance of the four algorithms when the power budget is varying. As we can see, when the budget increases, our objective function increases as expected.

For easy understanding, we visualize two charger placements and the corresponding allocated power levels generated by TCA for two instances of P^3 in Fig. 7. In Fig. 7a, there are a total of 9 candidate locations and 50 devices. TCA picks 6 of them, and the corresponding power levels are 4, 3, 1, 4, 1, and 3. As we mentioned in Eq. (4), the

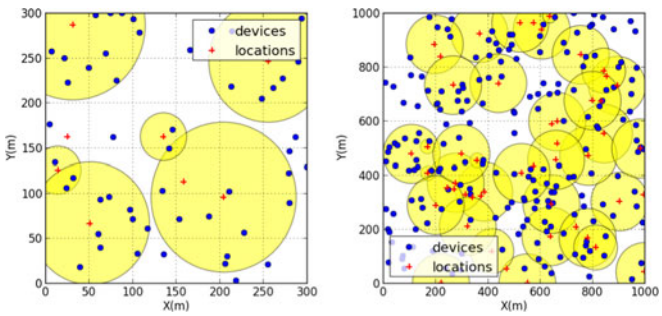

(a) A small instance (b) A large instance

Fig. 7. Visualization examples of SP^3.

maximum coverage distance is determined by the power level. In the figure, we use circle radius to indicate the allocated power level of a location. The charging quality (see Definition 1) of this solution is 0.77. In Fig. 7b, TCA picks 35 out of 50 candidate locations for charging 200 devices. The allocated power levels consist of four 1's, three 4's, and twenty-eight 6's, yielding a charging quality of 3.34.

We also conduct evaluations based on large instances of P^3. Fig. 8 depicts the performance of TCA, FLA, and RAN on large P^3 instances. Most of the findings from Fig. 6 still hold here. We would like to highlight that, in Fig. 8c, the increasing speed of the charging quality tends to slow down gradually, e.g., the increment of TCA between the first three consecutive groups are 0.21, 0.18, and 0.12. This is in accordance with the submodularity of the objective function.

Fig. 9 gives the comparison results on running time of TCA, FLA, and RAN. Remember that the worst case time complexity of TCA is $O(MN^3L^3)$, thus, it is expected that the running time of TCA increases as one of M, N, and L increases. An interesting observation is that, TCA runs faster on average when L increases. The main reason is that, when L increases, the number of iterations in each while-loop (i.e., lines 3-7 and 10-14) becomes smaller, which may shorten the running time.

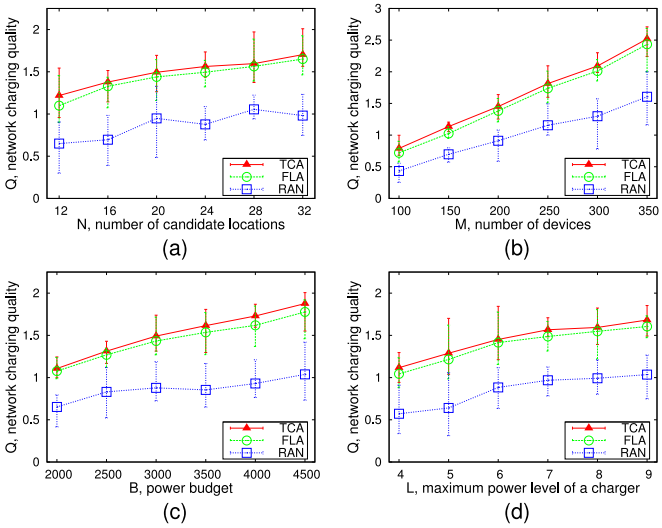

Fig. 8. Evaluation results on large instances of SP^3 (the default setting is $N = 20$, $M = 200$, $B = 3{,}000$, $L = 6$, and the side length of the 2-D plane is 1,000 m).

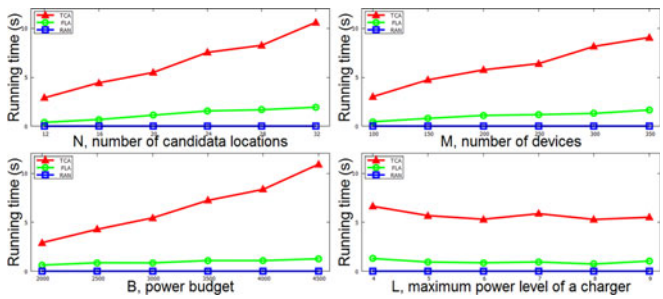

Fig. 9. Running time comparison in SP^3.

6.3 Results of MP^3

6.3.1 Setup

We evaluate the performance of tailored TCA on MP^3 instances. Most of the settings are similar to those in the last section, except the mobility model of mobile rechargeable devices. We consider two types of mobility models: *Random Waypoint (RWP)* and *Random Walk (RAW)*. In the RWP model, a device selects a random point within the 2-D area as its initial location, then it moves to a random waypoint and waits for a uniformly distributed time, and after that, moves to another random waypoint and repeats the process K times; in the RAW model, a device also selects a random point as its initial location, but at each location, the device randomly selects a direction and moves for a distance, which is called step length; if the border of the area is reached, select a new direction with the bouncing rule.

6.3.2 Results

Fig. 10 shows the results of different setups of small instances of MP^3. In general, *the gap between TCA and OPT is 4.4 percent at most and 3.5 percent on average*. Most of the findings are similar to those in the evaluations for SP^3. In Fig. 10c, when the maximum number K of grids that a device passes through increases, the charging quality of the four algorithms remains unchanged. This is because, the charging quality of one device is the weighted sum of its charging qualities over its positions. Fig. 10d presents the results

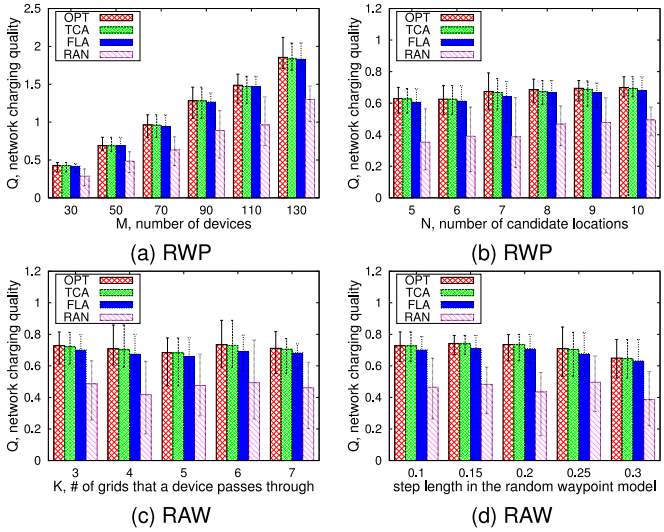

Fig. 10. Evaluation results on small instances of MP^3 (the default setting is $N = 8$, $M = 50$, $B = 800$, $L = 4$, $K = 5$, the side length of the 2-D plane is 300 m, and the step length is 0.2 $\times$ (2-D plane side length)).

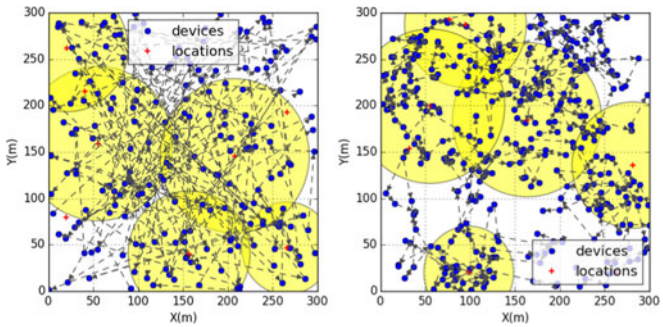

(a) RWP with $K = 4$ (b) RAW with $5 \leq K \leq 10$

Fig. 11. Visualization examples of MP^3. The trajectory of a device is represented by a series of blue circles connected by dashed lines.

with varying step lengths in the RAW mobility model. The x-axis shows the ratio of the step length over the the side length of the 2-D area. We observe that, when the step length increases, the average charging quality decreases. The main reason is, a large step length makes the positions of devices more disperse, making it difficult for chargers to cover these positions.

We also provide two visualization examples with two mobility models in Fig. 11. The trajectory of a device is presented by a set of blue circles connected by dashed lines. In both figures, there are in total 50 devices and 8 candidate locations; TCA picks 5 locations for placing chargers and the corresponding power allocations are 4, 4, 3, 3, and 2. We use circle radii to represent the coverage of a power level.

6.4 Results of Reconfiguration

In this section, we evaluate the performance of IAA, i.e., Algorithm 5, for CRP. In order to obtain the optimal solution by brute force, we use the same setting as that in the small instances of SP^3. We are interested in evaluating the effects of parameters F and δ.

In Fig. 12a, we fix $F = 400$ and see how the gap between OPT and IAA changes with varying δ. When δ increases, more devices enter or leave the target area; that is, given a fixed reconfiguration cost threshold, IAA cannot modify more power allocations as δ increases, leading to a lower charging quality.

In Fig. 12b, we fix $\delta = 0.3$ and see how the gap changes with varying F. We see that when the reconfiguration cost threshold increases, the gap shrinks. This is because, if more differences between $\mathbf{H}'$ and $\mathbf{H}$ are allowed, the amount of power levels IAA needs to modify decreases, thus, the charging quality loss due to the decrease of power levels in lines 5-6 in Algorithm 5 decreases. The evolution of the gap

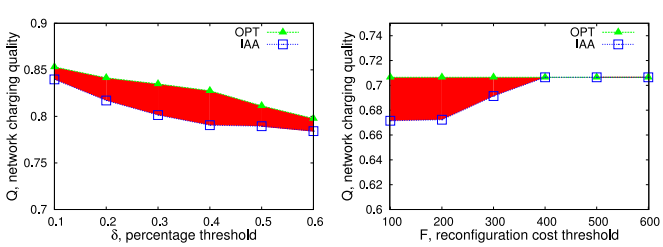

(a) F=400 (b) $\delta = 0.3$

Fig. 12. Evaluation results of IAA (the default setting is the same as that in Fig. 6).

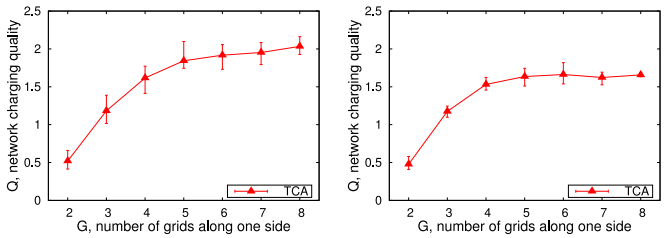

(a) Stationary devices (b) RAW

Fig. 13. The impact of G on the charging quality of TCA.

is also consistent with Theorem 4, in which the approximation ratio increases when F increases.

6.5 Results of More Candidate Locations

In this section, we consider the scenario with no preselected candidate locations. Fig. 13 shows the impact of G, i.e., the number of grids along one side of the square target area, on the charging quality returned by TCA. We observe that, when G increases, i.e., the number of grids in the area increases, the charging quality increases. This is reasonable, as more candidate locations provide more opportunities for picking better locations for placing chargers. We also find that, the growth speed decreases when G increases, implying an upper bound on the charging quality.

Fig. 14 shows an example of placement and allocation evolution when G increases. The settings are similar to those of Fig. 6. We find that, given the same set of rechargeable devices and their locations, increasing G indeed improves the overall charging quality Q. This evolution example also suggests that, the marginal increase of charging quality Q decreases as G increases, which is consistent with the observations in Fig. 13.

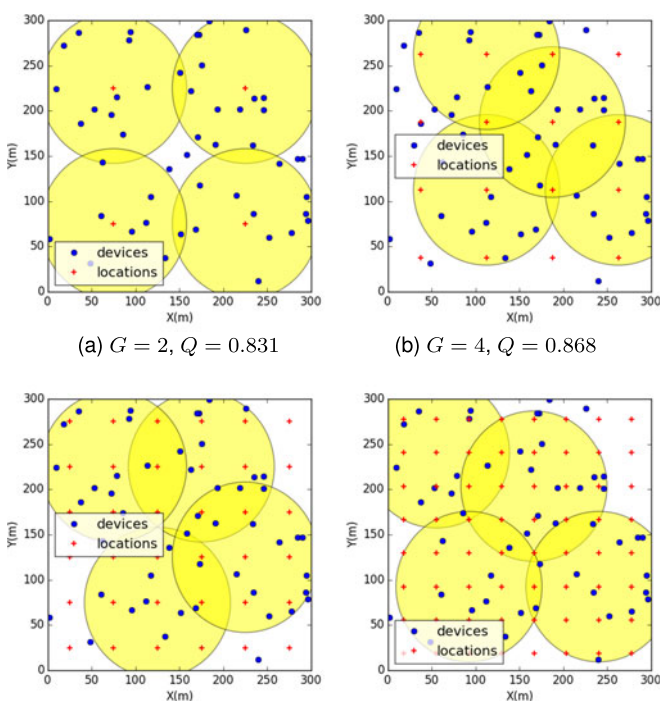

(a) $G = 2$, $Q = 0.831$ (b) $G = 4$, $Q = 0.868$

(c) $G = 6$, $Q = 0.911$ (d) $G = 8$, $Q = 0.912$

Fig. 14. Evolution of charger placement and power allocation as G increases.

In summary, the proposed algorithms perform very closely to OPT (the gap is no more than 4.5, 4.4, and 5.0 percent of OPT in SP^3, MP^3, and CRP, respectively), and outperforms the other baseline algorithms.

7 Conclusion

In this paper, we concentrate on the charging quality optimization for wireless charging service provision in 2-D areas. We first study SP^3 with stationary devices and devise an efficient approximation algorithm. We also show how to extend SP^3 via relaxing several assumptions, including mobile device, reconfiguration, and arbitrary candidate locations. Extensive evaluations confirm our theoretical analyses and show the proposed algorithms are very promising.

Acknowledgments

This work was supported in part by NSFC (61502224, 61472181, 61472185), CCF-Tencent Open Research Fund (AGR20160104), Jiangsu NSF (BK20151392, BK20151390), and the Collaborative Innovation Center of Novel Software Technology and Industrialization.

References

[1] A. Kansal, J. Hsu, S. Zahedi, and M. B. Srivastava, "Power management in energy harvesting sensor networks," *ACM Trans. Embedded Comput. Syst.*, vol. 6, no. 4, Sep. 2007, Art. no. 32.

[2] X. Jiang, J. Polastre, and D. Culler, "Perpetual environmentally powered sensor networks," in *Proc. ACM/IEEE 14th Int. Conf. Inf. Process. Sensor Netw.*, 2005, pp. 463–468.

[3] A. Cammarano, C. Petrioli, and D. Spenza, "Pro-energy: A novel energy prediction model for solar and wind energy-harvesting wireless sensor networks," in *Proc. IEE 12th Int. Conf. Mobile Ad Hoc Sensor Syst.*, 2012, pp. 75–83.

[4] A. Dunkels, F. Österlind, and Z. He, "An adaptive communication architecture for wireless sensor networks," in *Proc. ACM Conf. Embedded Netw. Sensor Syst.*, 2007, pp. 335–349.

[5] S. Bhattacharya, H. Kim, S. Prabh, and T. Abdelzaher, "Energy-conserving data placement and asynchronous multicast in wireless sensor networks," in *Proc. ACM 1st Int. Conf. Mobile Syst. Appl Serv.*, 2003, pp. 173–185.

[6] B. Tong, G. Wang, W. Zhang, and C. Wang, "Node reclamation and replacement for long-lived sensor networks," *IEEE Trans. Parallel Distrib. Syst.*, vol. 22, no. 9, pp. 1550–1563, Sep. 2011.

[7] A. Kurs, A. Karalis, R. Moffatt, J. D. Joannopoulos, P. Fisher, and M. Soljačić, "Wireless power transfer via strongly coupled magnetic resonances," *Sci.*, vol. 317, no. 5834, pp. 83–86, 2007.

[8] A. P. Sample, D. J. Yeager, P. S. Powledge, A. V. Mamishev, and J. R. Smith, "Design of an RFID-based battery-free programmable sensing platform," *IEEE Trans. Instrum. Meas.*, vol. 57, no. 11, pp. 2608–2615, 2008.

[9] Androidcentral. (2015). [Online]. Available: http://www.androidcentral.com/these-android-phones-can-handle-wireless-charging/

[10] Tesla motors. (2015). [Online]. Available: http://www.teslamotors.com/

[11] SHARP. (2015). [Online]. Available: http://www.friendsofcrc.ca/Projects/SHARP/sharp.html

[12] Wireless charging market. (2015). [Online]. Available: http://www.marketsandmarkets.com/PressReleases/wireless-charging.asp

[13] Y. Peng, Z. Li, W. Zhang, and D. Qiao, "Prolonging sensor network lifetime through wireless charging," in *Proc. IEEE 31st Real-Time Syst. Symp.*, 2010, pp. 129–139.

[14] Y. Shi, L. Xie, Y. Hou, and H. Sherali, "On renewable sensor networks with wireless energy transfer," in *Proc. IEEE Conf. Inf. Comput. Commun.*, 2011, pp. 1350–1358.

[15] S. He, J. Chen, F. Jiang, D. K. Yau, G. Xing, and Y. Sun, "Energy provisioning in wireless rechargeable sensor networks," in *Proc. IEEE Conf. Inf. Comput. Commun.*, 2011, pp. 2006–2014.

[16] S. Zhang, J. Wu, and S. Lu, "Collaborative mobile charging," *IEEE Trans. Comput.*, vol. 64, no. 3, pp. 654–667, Mar. 2015.

[17] L. Fu, P. Cheng, Y. Gu, J. Chen, and T. He, "Minimizing charging delay in wireless rechargeable sensor networks," in *Proc. IEEE Conf. Inf. Comput. Commun.*, 2013, pp. 2922–2930.

[18] H. Dai, Y. Liu, G. Chen, X. Wu, and T. He, "Scape: Safe charging with adjustable power," in *Proc. 37th IEEE Int. Conf. Distrib. Comput. Syst.*, 2014, pp. 439–448.

[19] WPC. (2015). [Online]. Available: http://www.wirelesspowerconsortium.com/

[20] PMA. (2015). [Online]. Available: http://www.powermatters.org/

[21] A4WP. (2015). [Online]. Available: http://a4wppmamerge.wwwssr6.supercp.com/

[22] S. Zhang, Z. Qian, F. Kong, J. Wu, and S. Lu, "P^3: Joint optimization of charger placement and power allocation for wireless power transfer," in *Proc. IEEE Conf. Inf. Comput. Commun.*, 2015, pp. 2344–2352.

[23] V. V. Vazirani, *Approximation Algorithms*. Berlin, Germany: Springer, 2003.

[24] M. Cheney, J. Glenn, and R. Uth, *Tesla: Master Lightning*. New York, NY, USA: Barnes & Noble Publishing, 1999.

[25] WiPoT. (2015). [Online]. Available: http://www.wipot.jp/english/

[26] N. Shinohara, *Simultaneous WPT and Wireless Commun. with TDD Algorithm at Same Frequency Band*. Berlin, Germany: Springer, 2016, pp. 211–229.

[27] M. Zhao, J. Li, and Y. Yang, "Joint mobile energy replenishment and data gathering in wireless rechargeable sensor networks," in *Proc. ACM Proc. 23rd Int. Teletraffic Congress*, 2011, pp. 238–245.

[28] C. Wang, J. Li, F. Ye, and Y. Yang, "NETWRAP: An NDN based real-time wireless recharging framework for wireless sensor networks," *IEEE Trans. Mobile Comput.*, vol. 13, no. 6, pp. 1283–1297, Jun. 2014.

[29] S. Nikoletseas, Y. Yang, and A. Georgiadis, *Wireless Power Transfer Algorithms, Technologies and Applications in Ad Hoc Communication Networks*. Berlin, Germany: Springer, 2016.

[30] B. Tong, Z. Li, G. Wang, and W. Zhang, "How wireless power charging technology affects sensor network deployment and routing," in *Proc. 37th IEEE Int. Conf. Distrib. Comput. Syst.*, 2010, pp. 438–447.

[31] Z. Li, Y. Peng, W. Zhang, and D. Qiao, "Study of joint routing and wireless charging strategies in sensor networks," in *Proc. Int. Conf. Wireless Algorithms Syst. Appl.*, 2010, pp. 125–135.

[32] Y. Shu, et al., "Near-optimal velocity control for mobile charging in wireless rechargeable sensor networks," *IEEE Trans. Mobile Comput.*, vol. 15, no. 7, pp. 1699–1713, Jul. 2016.

[33] L. Xie, Y. Shi, Y. T. Hou, W. Lou, H. D. Sherali, and S. F. Midkiff, "On renewable sensor networks with wireless energy transfer: The multi-node case," in *Proc. IEEE 11th Annu. IEEE Int. Conf. Sensing Commun. Netw.*, 2012, pp. 10–18.

[34] J. Wu, "Collaborative mobile charging and coverage," *J. Comput. Sci. Technol.*, vol. 29, no. 4, pp. 550–561, 2014.

[35] L. Fu, L. He, P. Cheng, Y. Gu, J. Pan, and J. Chen, "ESync: Energy synchronized mobile charging in rechargeable wireless sensor networks," *IEEE Trans. Veh. Technol.*, vol. 65, no. 9, pp. 7415–7431, Sept. 2016.

[36] W. Xu, W. Liang, X. Lin, and G. Mao, "Efficient scheduling of multiple mobile chargers for wireless sensor networks," *IEEE Trans. Veh. Technol.*, vol. 65, no. 9, pp. 7670–7683, Sept. 2016.

[37] S. Zhang, Z. Qian, J. Wu, F. Kong, and S. Lu, "Optimizing itinerary selection and charging association for mobile chargers," *IEEE Trans. Mobile Comput.*, vol. 16, no. 10, pp. 2833–2846, Oct. 2017.

[38] N. Patwari, A. O. Hero, M. Perkins, N. S. Correal, and R. J. O'dea, "Relative location estimation in wireless sensor networks," *IEEE Trans. Signal Process.*, vol. 51, no. 8, pp. 2137–2148, 2003.

[39] G. L. Nemhauser, L. A. Wolsey, and M. L. Fisher, "An analysis of approximations for maximizing submodular set functions–I," *Math. Program.*, vol. 14, no. 1, pp. 265–294, 1978.

[40] D. Yang, X. Fang, and G. Xue, "ESPN: Efficient server placement in probabilistic networks with budget constraint," in *Proc. IEEE Conf. Inf. Comput. Commun.*, 2011, pp. 1269–1277.

[41] J. Leskovec, A. Krause, C. Guestrin, C. Faloutsos, J. VanBriesen, and N. Glance, "Cost-effective outbreak detection in networks," in *Proc. ACM 10th ACM SIGKDD Int. Conf. Knowl. Discovery Data Mining*, 2007, pp. 420–429.

Sheng Zhang received the BS and the PhD degrees from Nanjing University, in 2008 and 2014, respectively. Currently, he is an assistant professor in the Department of Computer Science and Technology, Nanjing University. He is also a member of the State Key Laboratory for Novel Software Technology. His research interests include cloud computing and mobile networks. To date, he has published more than 40 papers, including those which appeared in the *IEEE Transactions on Mobile Computing*, the *IEEE Transactions on Parallel and Distributed Systems*, the *IEEE Transactions on Computers*, ACM MobiHoc, IEEE ICDCS, and IEEE INFOCOM. He received the Best Paper Runner-Up Award from IEEE MASS 2012. He is a member of the IEEE.

Zhuzhong Qian received the PhD degree from Nanjing University, in 2007. He is an associate professor in the Department of Computer Science and Technology, Nanjing University. His current research interests include distributed systems and data center networking. He has published more than 40 papers in referred journals and conferences, including the *IEEE Transactions on Parallel and Distributed Systems*, INFOCOM, and IPDPS. He is a member of the IEEE.

Jie Wu (F'09) is the chair and a Laura H. Carnell professor in the Department of Computer and Information Sciences at Temple University. He is also an Intellectual Ventures endowed visiting chair professor with the National Laboratory for Information Science and Technology, Tsinghua University. Prior to joining Temple University, he was a program director in the National Science Foundation and was a distinguished professor with Florida Atlantic University. His current research interests include mobile computing and wireless networks, routing protocols, cloud and green computing, network trust and security, and social network applications. He regularly publishes in scholarly journals, conference proceedings, and books. He serves on several editorial boards, including the *IEEE Transactions on Service Computing* and the the *Journal of Parallel and Distributed Computing*. He was general co-chair/chair of IEEE MASS 2006, IEEE IPDPS 2008, IEEE ICDCS 2013, and ACM MobiHoc 2014, as well as program co-chair of IEEE INFOCOM 2011 and CCF CNCC 2013. He was an IEEE Computer Society Distinguished Visitor, ACM Distinguished Speaker, and chair for the IEEE Technical Committee on Distributed Processing (TCDP). He is the recipient of the 2011 China Computer Federation (CCF) Overseas Outstanding Achievement Award. He is a CCF Distinguished Speaker and a fellow of the IEEE.

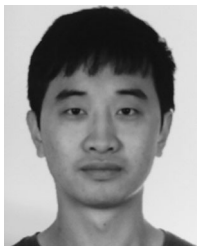

Fanyu Kong received the BS and the MS degrees from Nanjing University, in 2013 and 2016, respectively. He is now with Ant Financial, China. His research interests include load balancing and failure monitoring in public clouds via openstack.

Sanglu Lu received the BS, MS, and the PhD degrees from Nanjing University, in 1992, 1995, and 1997, respectively, all in computer science. She is currently a professor in the Department of Computer Science and Technology and the State Key Laboratory for Novel Software Technology. Her research interests include distributed computing, wireless networks, and pervasive computing. She has published more than 80 papers in referred journals and conferences in the above areas. She is a member of IEEE.